Supplementary Information (SI) for Journal of Materials Chemistry A.

Supporting Information

Viscoelasticity-Controllable Dynamic Borate Polydimethylsiloxane Network For Enhancing Energy Dissipation of Elastomers

Fu-Long Gong[1,2], Shuang Long[1,2], Wenqing Lv[1,2], Xiaotong Shu[1,2], Bin Huang[1], Pingping Lou[1], Hua-Feng Fei[1,2], and Zhijie Zhang[1]*

[1]Key Laboratory of Science and Technology on High-tech Polymer Materials, Institute of Chemistry, Chinese Academy of Sciences, Beijing, 100190, P. R. China.

[2]School of Chemical Sciences, University of Chinese Academy of Sciences, Beijing 100049, P. R. China.

*Corresponding Author: Hua-Feng Fei (feihuafeng@iccas.ac.cn)

Experimental Procedures

1.1 Materials and Methods

Dihydroxy-terminated poly(dimethylsiloxane) (PDMS-OH，weight-average molecular masses M_w = 1.2k，36k，49k） was obtained from Gelest Inc. Dihydroxy-terminated poly(dimethylsiloxane) (PDMS-OH，M_w = 4.2 k）was obtained from Thermo Scientific. Dihydroxy-terminated poly(dimethylsiloxane) (PDMS-OH，M_w = 18k，110k）was obtained from Sigma-Aldrich. Dihydroxy-terminated poly(dimethylsiloxane) (PDMS-OH，M_w = 77 k）was obtained from Macklin. 1,4-Phenylenebisboronic acid (PDBA), and boric acid (BA) was obtained from Accela and J&K Chemical Co., Ltd., respectively. Ethanol and Isopropanol was purchased from Concord Technology (Tianjin) Co., Ltd. PDMS prepolymers (dimethylhydrogen siloxane, dimethylvinyl-terminated dimethylsiloxane) and the Pt catalyst was homemade in our lab. All reagents were used as received.

1.2 Synthesis of the Poly 1,4-phenylenediborosiloxane (PPDBS) Networks[1]：

Typically, 1,4-Phenylenebisboronic acid (PDBA) was weighed out in a stoichiometric ratio of 1:2 of cross-linker to dihydroxy-terminated poly(dimethylsiloxane) and dissolved in isopropanol. Then, the calculated amount of PDMS-OH was added into the above solution and stirred for 2 h at 60 °C to form oligomeric products. The reaction mixture was then heated at 120 °C to remove the water condense and isopropanol. The resulted sample was dried after 12 h of mechanical stirring under vacuum to obtain PPDBS Networks. A series of PPDBS were obtained by changed the molecular weight of PDMS-OH as shown in Table S1 and Table S2. The PPDBS samples were kept in the drying oven at room temperature before use.

1.3 Synthesis of the Polyborosiloxane (PBS) Networks[2]：

Typically, boronic acid (BA) was weighed out in a stoichiometric ratio of 1:1.5 of cross-linker to dihydroxy-terminated poly(dimethylsiloxane) and dissolved in ethanol. Then, the calculated amount of PDMS-OH was added into the above solution and stirred for 2 h at 60 °C to form oligomeric products. The reaction mixture was then heated at 120 °C to remove the water condense and ethanol，and the experiment was stopped after 12 h of mechanical stirring under vacuum to obtain PBS Networks. A series of PBS were obtained by changed the Molecular Weight of PDMS-OH as shown in Table S1. The PBS samples were kept in the drying oven at room temperature before use.

1.4 Preparation of the PDMS elastomer:

The PDMS precursors and the Pt catalyst (0.1 wt%) were thoroughly mixed in a centrifugal mixer (DAC 330-100 SE) to ensure uniform dispersion and eliminate air bubbles. Then the mixture was poured into the Teflon model and cured at 120 °C for 2 h to obtain PDMS elastomer.

1.4 Preparation of the PDMS/PPDBS double-network elastomers (SSEs):

Firstly, the PPDBS and the Pt catalyst (0.1 wt%) was added into the PDMS precursors and were mixed together, then the mixture was poured into the Teflon model and cured at 120 °C for 2 h to obtain PDMS/PPDBS double network elastomers (SSEs). A series of SSE-x-11w (x = the weight fraction of the PPDBS) were obtained by changed the content of the PPDBS-110k as shown in Table S3, and were named by SSE-0.4-110k, SSE-0.5-110k, SSE-0.66-110k, SSE-0.75-110k, SSE-0.8-110k. A series of SSE-x-4.2k were obtained by changed the content of the PPDBS4200 as shown in Table S3, and were named by SSE-0.2-4.2k, SSE-0.4-4.2k, SSE-0.5-4.2k, SSE-0.6-4.2k. And a series of SSEs with same content of the permanent crosslinked network (PDMS) were obtained by changed the structures of the PPDBS as shown in Table S4, and named by SSE-0.5-4.2k, SSE-0.5-18k, SSE-0.5-49K, SSE-0.5-77K, SSE-0.5-110K..

1.5 Preparation of the PDMS/PBS double network-elastomers (SSE-x-PBS):

The PDMS/PBS SSEs were prepared by the same method described above while PPDBS4200 was replaced by PBS4200 as shown in Table S3, and named by SSE-0.2-PBS, SSE-0.4-PBS, SSE-0.5-PBS, SSE-0.6-PBS.

Characterization:

Structural Characterization: All ^{11}B MAS NMR spectra were obtained on a Bruker

NEO 600 SB spectrometer with magic angle spinning at 12 kHz. Chemical shifts are reported in parts per million (ppm) downfield with respect to $BF_3.Et_2O$.

FTIR-ATR measurements were performed using a Bruker Tensor-27 FTIR spectrometer from 4000 to 550 cm^{-1}.

Gel permeation chromatography (GPC) was performed in Toluene at 40 ºC with a flow rate of 1 mL/min on a Waters Alliance HPLC system equipped with a 515 pump and a 2410 refractive index detector.

The microscopic morphology was obtained by scanning electron microscope (SEM, Hitachi SU 8020).

Thermal analysis test: Decomposition temperature (T_d) of thoroughly dried polymer samples were measured by thermogravimetric analyzer (TGA) on METTLER TOLEDO TG2, METTLER Instrument. The samples were heated from 50 °C to 800 °C with a rate of 10 °C min^{-1}. T_d values were obtained from wt% vs. temperature (°C) plots and defined by the temperature of 5% weight loss.

Differential scanning calorimetry (DSC) test: Differential scanning calorimetry (DSC) experiments were conducted using a METTLER TOLEDO DS3 Instruments by using Tzero Aluminum pans under the nitrogen. The samples were heated from −150 °C or -140 °C to 40 °C with a rate of 10 °C min^{-1}.

Transmittance tests: Lambda 1050+ ultraviolet/visible/near infrared spectrometer was used to characterize light transmittance of 2-mm thick specimens.

Mechanical tests: Tensile stress/strain tests were tested at room temperature using Instron 5565 of British Instron Ltd. Instrument. The sample was cut into a dumbbell shape（50 mm × 4mm × 2mm）according to GB/T 528-2009, and 3 dumbbell-shaped samples were stretched at ambient temperature until break for each group of samples, and the average values with standard error were calculated. Unless otherwise specified, the rate of stretching test was 200 mm/min. Cyclic tensile tests were tested on the Instron 5565 tensile tester with the speed of 100 mm/min.

Mechanical compress experiments were performed using a TA.XTC-20 Texture Analyzer (Shanghai BosinTech). The samples were cylindrical with a diameter of 10 mm and a thickness of 5 mm. Unless otherwise specified, the rate of compressing test was 100 mm/min.

Rheological measurement: Rheological experiments were carried out using a HAAKE MARS 60 modular rheometer (Thermo Scientific) equipped with a temperature control system. Parallel plates with a diameter of 20 mm were used for the rheological experiments. Samples were prepared in the form of disks with a thickness of 2 mm. Dynamic oscillatory frequency sweeps from 0.01 to 50 Hz were performed with fixed strain of 0.1% at 25 °C. The temperature-dependent G′/G″ curves were measured at a constant frequency of 1 Hz over a temperature range of -20 to 150 °C with a heating rate of 5 °C min^{-1}.

Oscillatory frequency sweeps ranging from 0.1 to 50 Hz are measured in a range of temperatures T= 0 –150 °C. The master curve is followed by the time–temperature superposition principle and obtained by applying horizontal shift factors on the moduli curves at different temperatures. The temperature dependence of the time-temperature superposition shifting factors (a_T) was determined using the Williams-Landel-Ferry (WLF) formula. The horizontal shift factors (a_T) as a function of temperature can be fitted using the Arrhenius equations.

Large amplitude oscillatory shear (LAOS) tests of the materials with 2 mm height were measured by HAAKE MARS 60 modular rheometer (Thermo Scientific) at 25 °C.[3] In LAOS tests, a sinusoidal alternating stress (18 kPa) at a frequency of 1 Hz was applied to the sample. The hysteresis loop area represented the mechanical energy that converted to heat each cycle, and the energy dissipation was calculated through the circular area.

Falling-ball impact tests. The sample was stuck on a holder connected with a mechanical sensor. A steel ball (30 g) freely fell from the setting height, hitting the samples with the thicknesses of 2 mm. Force–time curve was analyzed from the collected data in the bottom of sample. The frequency signal was 200 kHz.

SI Fig.s and Tables

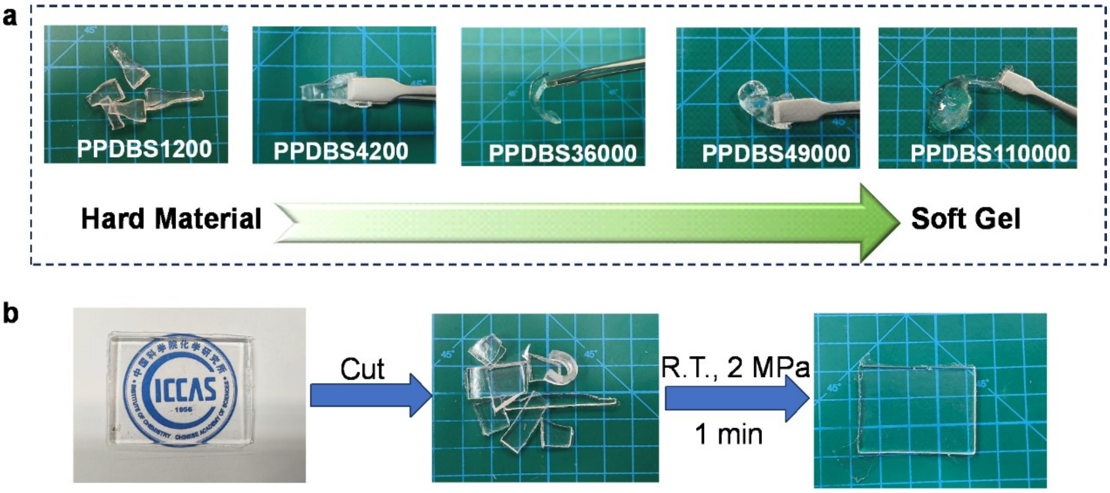

Fig. S1 (a). Photographs of the PPDBS networks. All the samples are optically transparent. (b). Reprocessability of the PPDBS Networks.

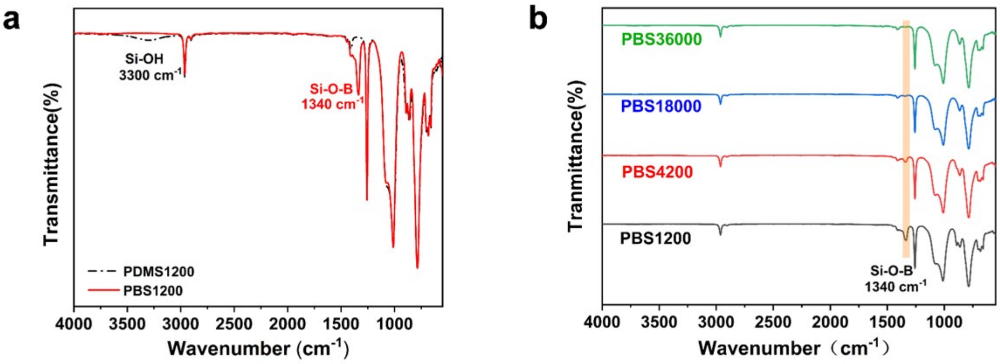

Fig. S2 (a). FT-IR spectra of PDMS1200 and PBS1200. (b). FT-IR spectra of PBS1200, PBS4200, PBS18000, PBS36000.

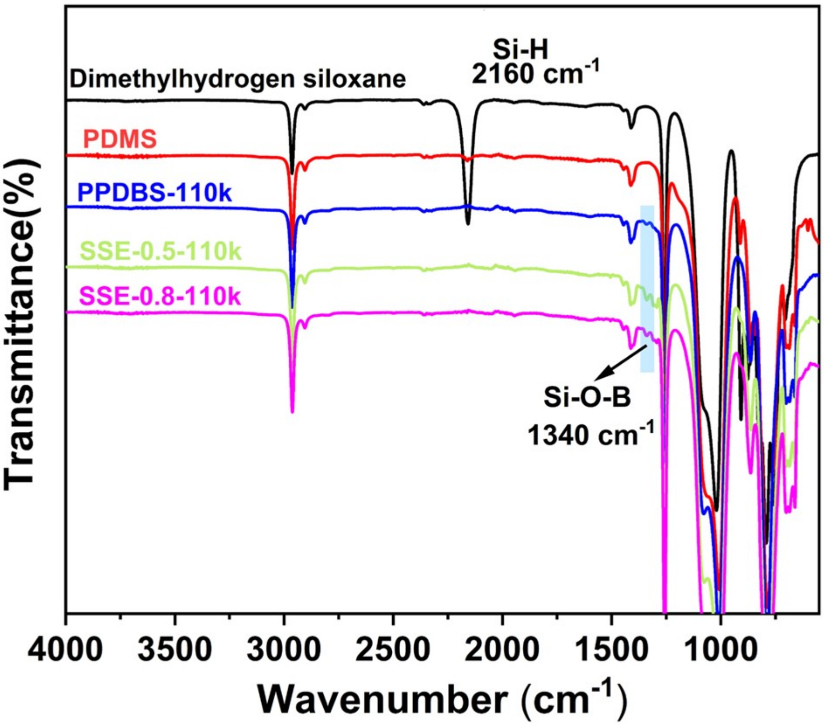

Fig. S3 FT-IR spectra of dimethylhydrogen siloxane, PDMS, PPDBS110k and SSE-x-110k. The absence of signals at the 2160 cm^{-1} and the presence of a Si-O-B bond at 1340 cm^{-1}, implying the formation of the PDMS/PPDBS double-network elastomer.

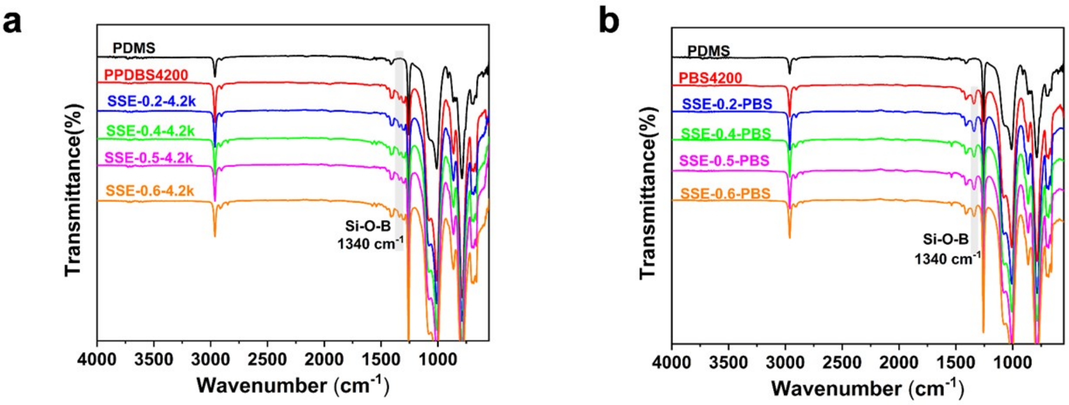

Fig. S4 (a). FT-IR show the formation of DN-x-4.2k through one-pot reaction. (b). FT-IR show the formation of DN-x-PBS through one-pot reaction.

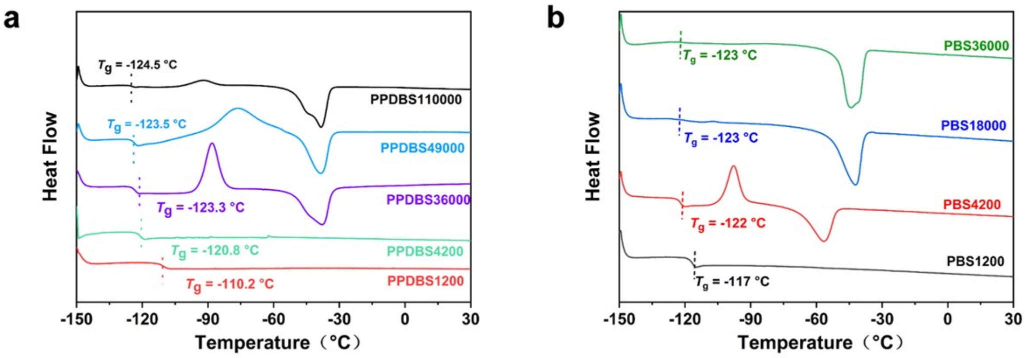

Fig. S5 (a). DSC curves for PPDBS with different crosslink density. (b). DSC curves for PBS with different crosslink density

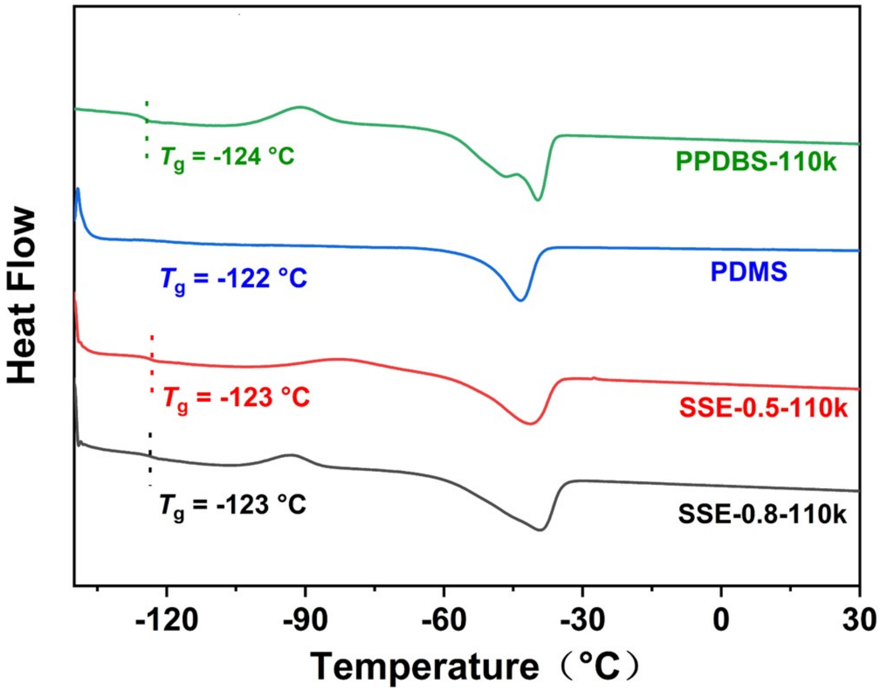

Fig. S6 DSC curves for PPDBS-110k, PDMS, DN-0.5-110k, DN-0.8-110k.

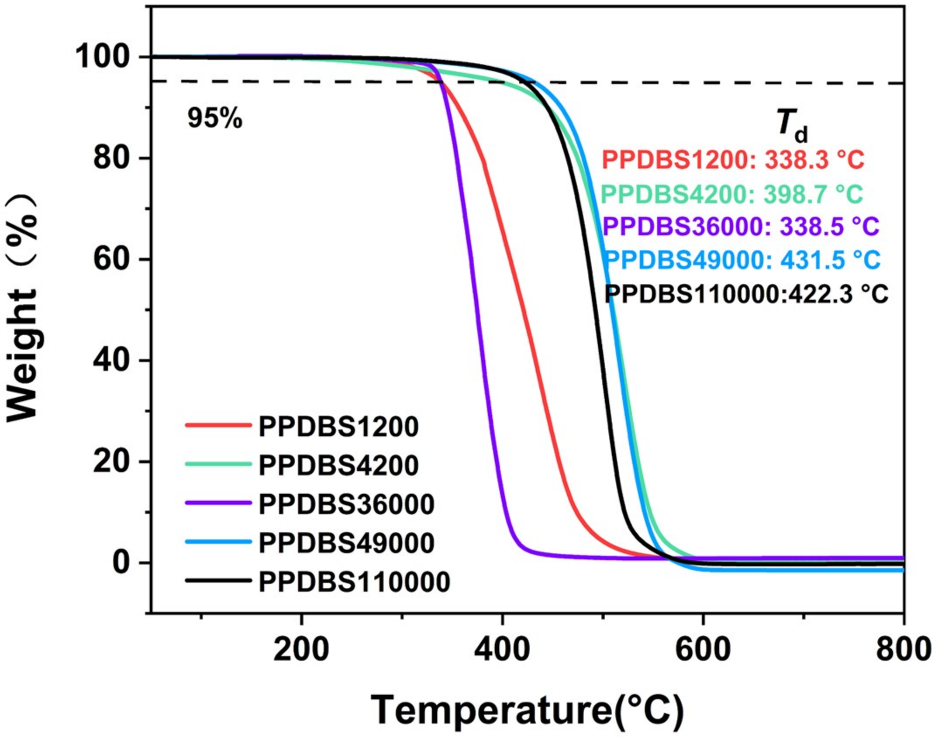

Fig. S7 TGA curves for PPDBS1200, PPDBS4200, PPDBS36000, PPDBS49000 and PPDBS110000.

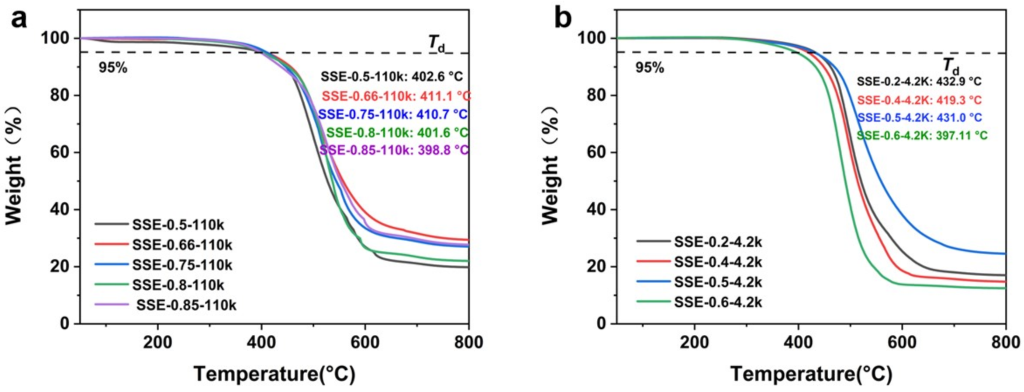

Fig. S8 (a). TGA curves for SSE-x-110k (x = 0.5, 0.66, 0.75, 0.8 and 0.85). (b). TGA curves for SSE-x-4.2k (x = 0.2, 0.4, 0.5 and 0.6).

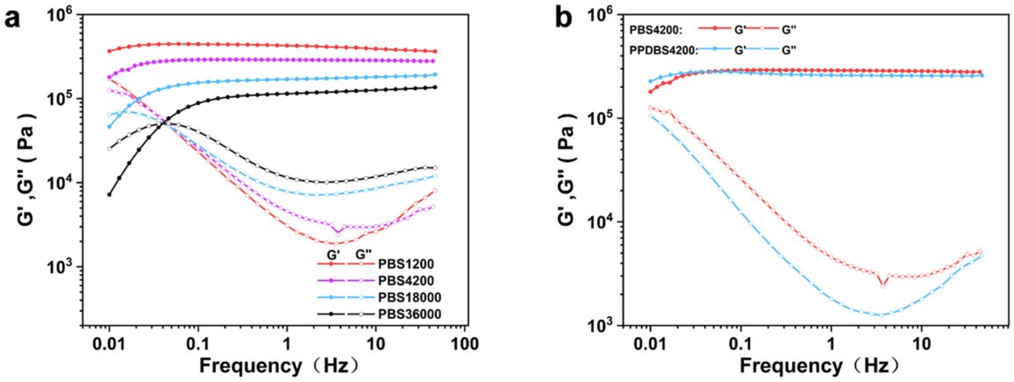

Fig. S9 (a). Frequency−sweep rheological curves of PBSx from 0.01 to 50 Hz. (b). Frequency-sweep rheological curves of PBS4200 and PPDBS4200. The plateau moduli of PBS increased with increasing crosslinking density, which is similar with PPDBS.

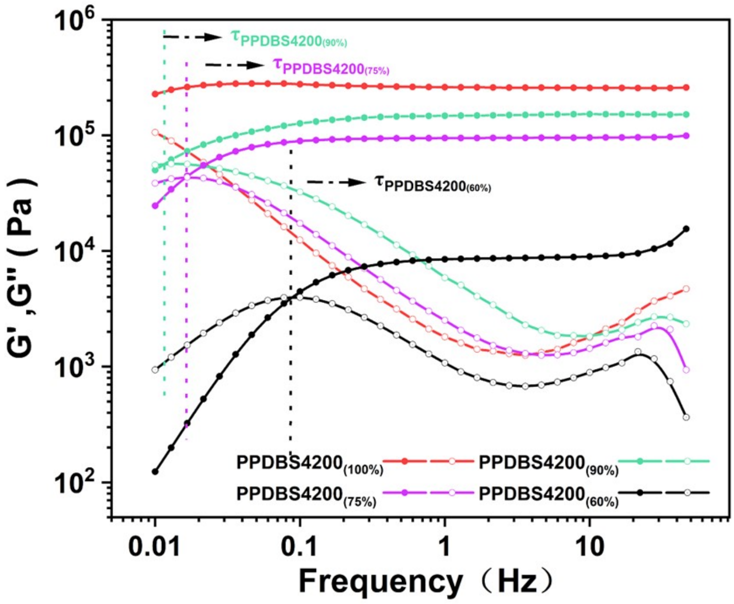

Fig. S10 Frequency−sweep rheological curves of PPDBS4200(100%), PPDBS(90%), PPDBS(75%) and PPDBS(60%). PPDBS4200 samples with 90%, 75% and 60% OH group reacted with PDBA were synthesized to verify the relationship between the characteristic relaxation time and free OH groups.

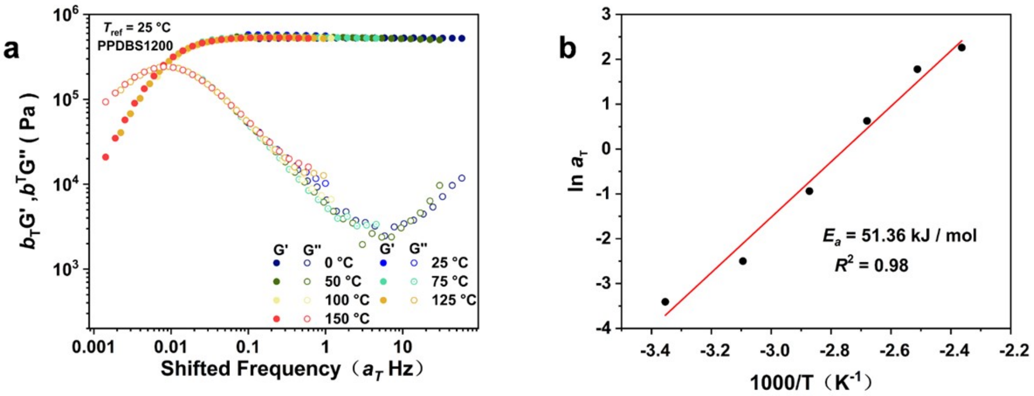

Fig. S11 (a). Rheological master curves of PPDBS1200 at T_{ref} = 25 °C. (b). plots of horizontal shift factors a_T as a function of inverse temperature with the Arrhenius type fit to determine the activation energy (E_a) for PPDBS1200.

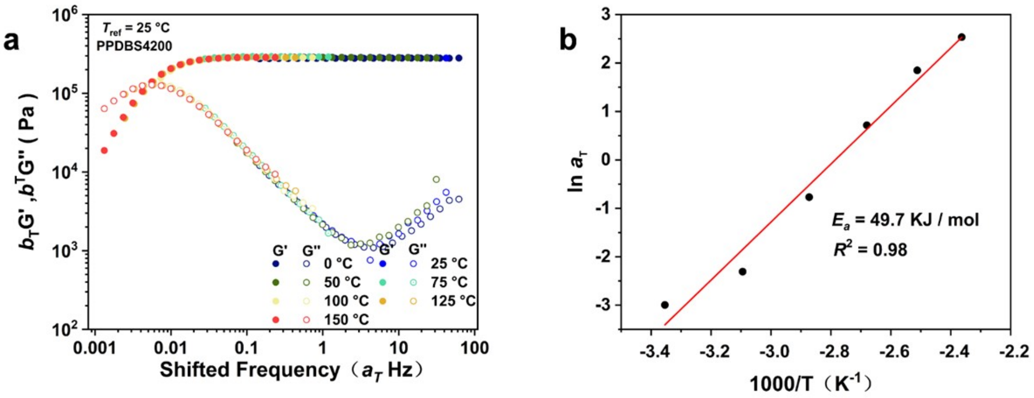

Fig. S12 (a). Rheological master curves of PPDBS4200 at T_{ref} = 25 °C. (b). plots of horizontal shift factors a_T as a function of inverse temperature with the Arrhenius type fit to determine the activation energy (E_a) for PPDBS4200.

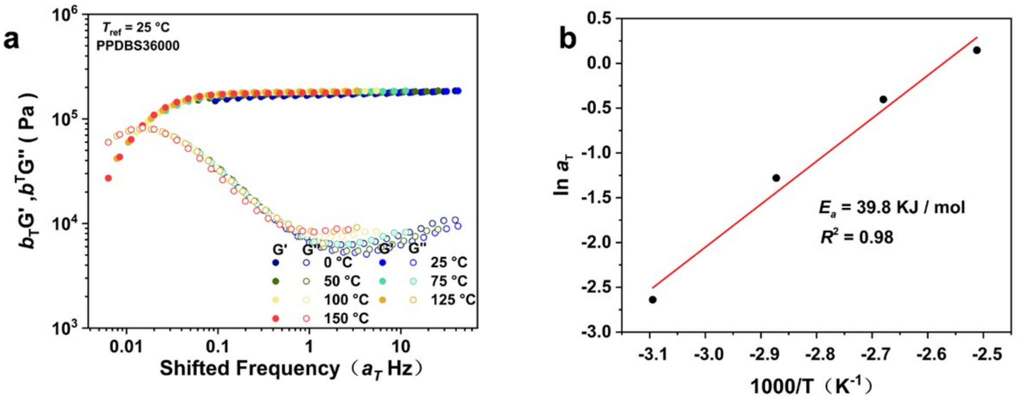

Fig. S13 (a). Rheological master curves of PPDBS36000 at T_{ref} = 25 °C. (b). plots of horizontal shift factors a_T as a function of inverse temperature with the Arrhenius type fit to determine the activation energy (E_a) for PPDBS36000.

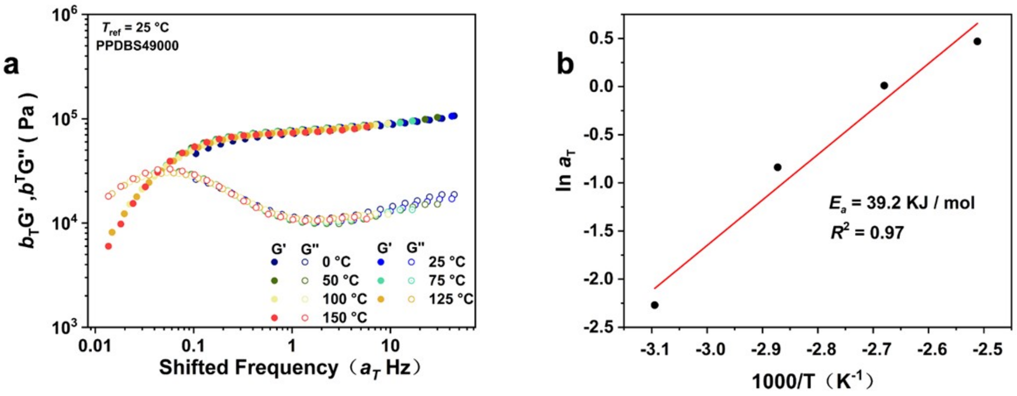

Fig. S14 (a). Rheological master curves of PPDBS49000 at T_{ref} = 25 °C. (b). plots of horizontal shift factors a_T as a function of inverse temperature with the Arrhenius type fit to determine the activation energy (E_a) for PPDBS49000.

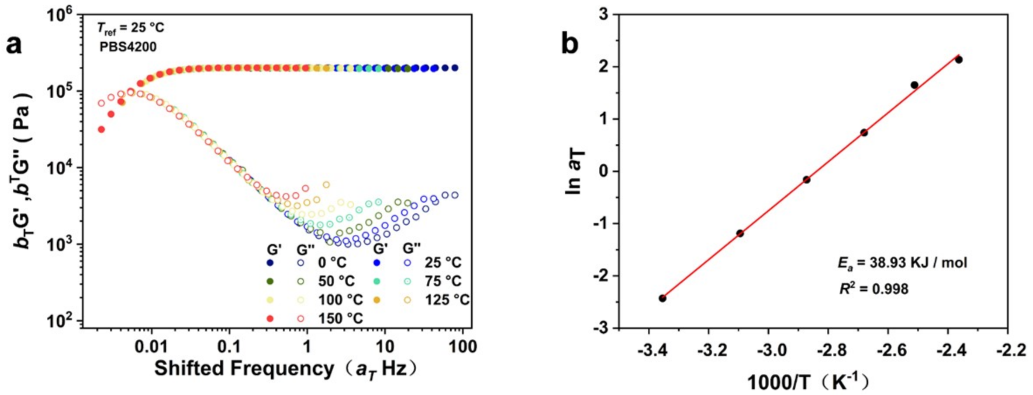

Fig. S15 (a). Rheological master curves of PBS4200 at T_{ref} = 25 °C. (b). plots of horizontal shift factors a_T as a function of inverse temperature with the Arrhenius type fit to determine the activation energy (E_a) for PBS4200.

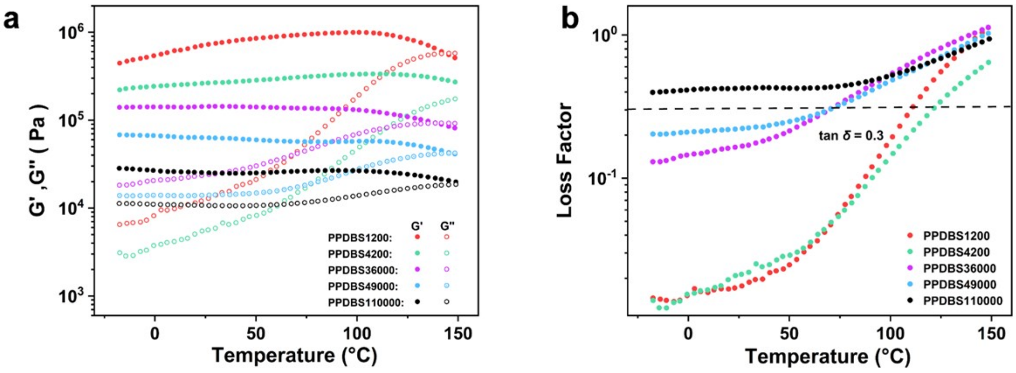

Fig. S16 Temperature−sweep rheological curves of PPDBSx from -20 to 150 °C. Temperature dependence of **G’, G’’ (a)** and **loss factor (b)** for PPDBSx.

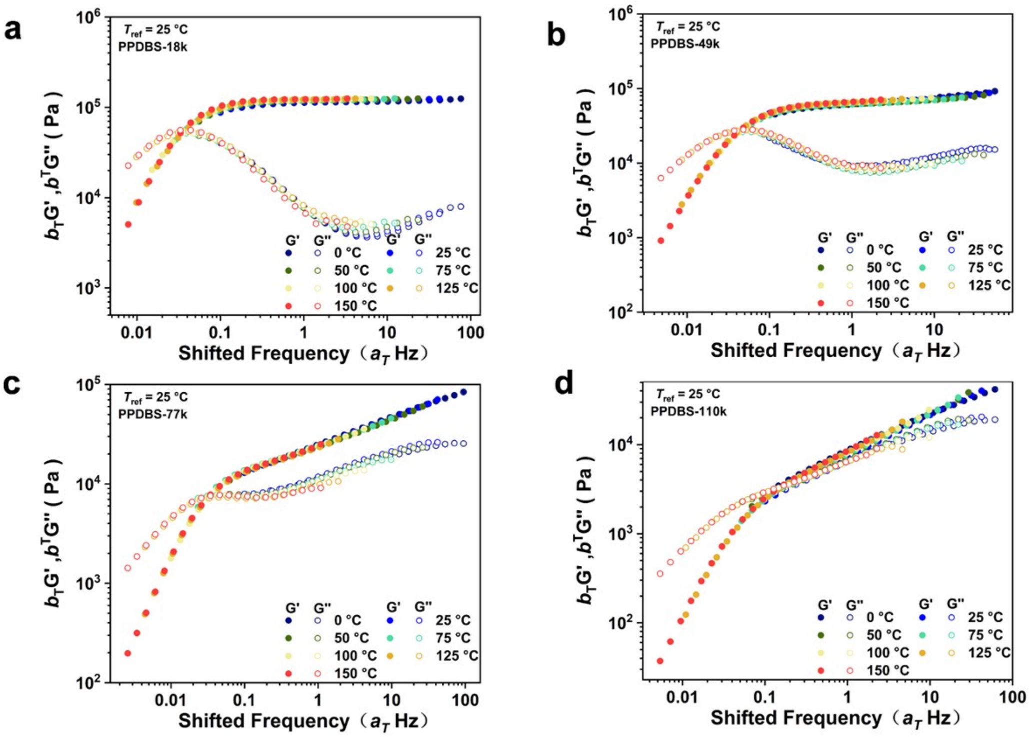

Fig. S17 (a). Rheological master curves of PPDBS-18k at T_{ref} = 25 °C. (b). Rheological master curves of PPDBS-49k at T_{ref} = 25 °C. (c). Rheological master curves of PPDBS-77k at T_{ref} = 25 °C. (d). Rheological master curves of PPDBS-110k at T_{ref} = 25 °C.

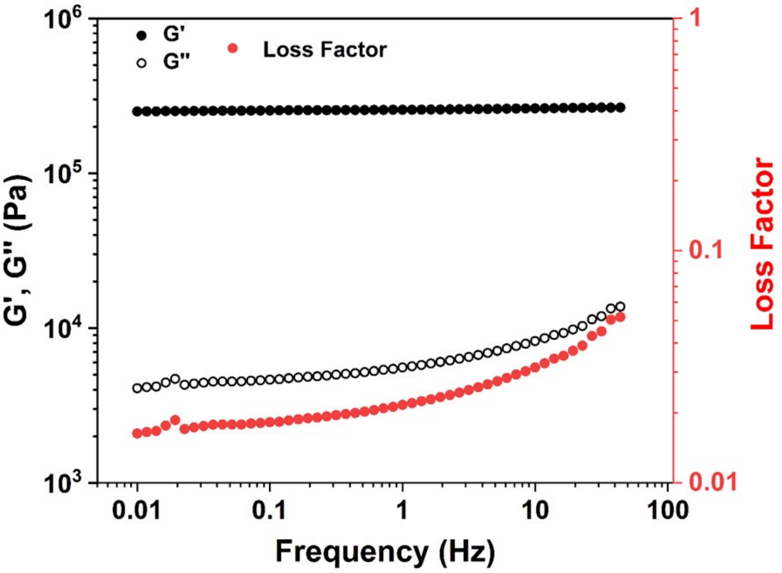

Fig. S18 Frequency−sweep rheological curves of PDMS from 0.01 to 50 Hz.

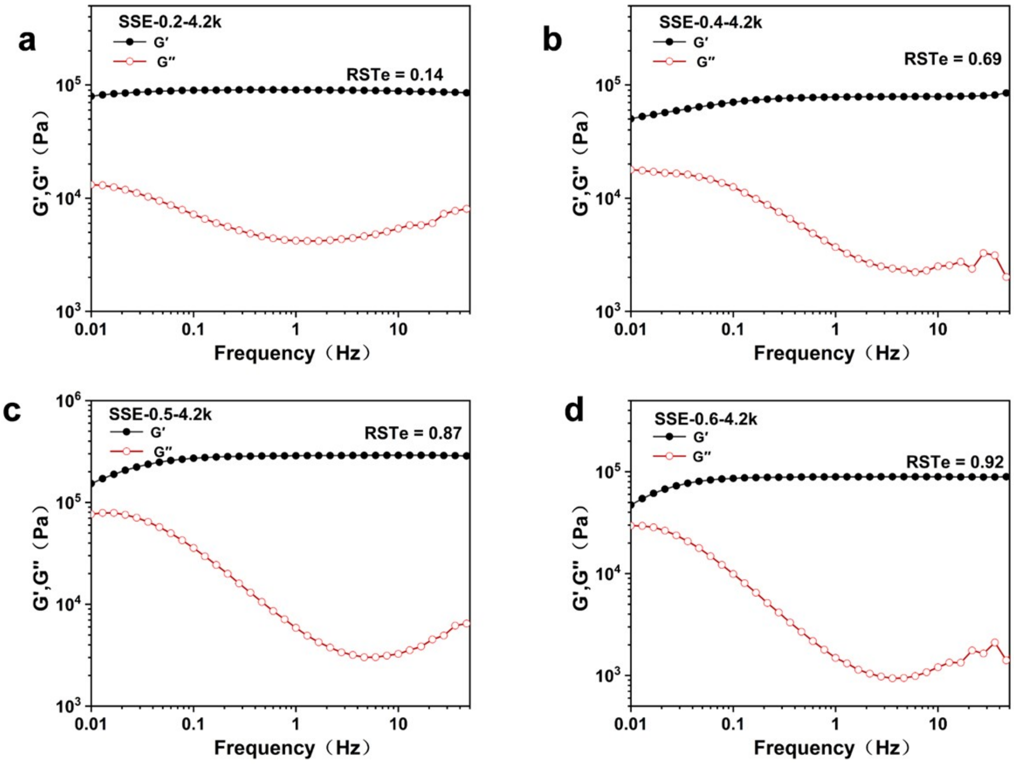

Fig. S19 Frequency−sweep rheological curves of SSE-0.2-4.2k (a), SSE-0.4-4.2k (b), SSE-0.5-4.2k (c) and SSE-0.6-4.2k (d) from 0.1 to 50 Hz. The RSTe values of the SSE-x-4.2k increased as the PPDBS4200 content rose from 20% to 60% (w/w), confirmed that the introduction of PPDBS imparts shear-stiffening behavior to the SSEs.

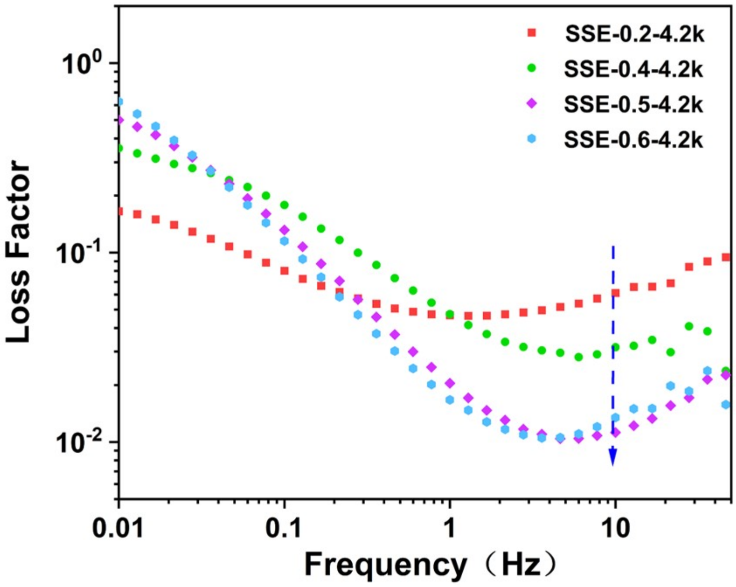

Fig. S20 Loss factor curves of SSE-0.2-4.2k, SSE-0.4-4.2k, SSE-0.5-4.2k and SSE-0.6-4.2k.

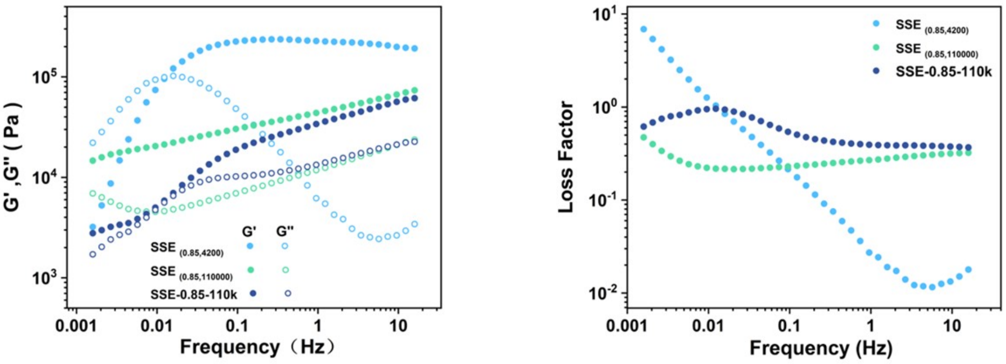

Fig. S21: The frequency−sweep rheological curves of SSE$_{(0.85,4200)}$, SSE$_{(0.85,110000)}$ and SSE-0.85-110k

We have synthesized the SSE samples with a content of 85 wt% for both PPDBS4200 and PPDBS110000, which have designated as SSE$_{(0.85,4200)}$ and SSE$_{(0.85,110000)}$, respectively. For SSE$_{(0.85,4200)}$, G' is much larger than G'' at higher frequency range due to the dense dynamic crosslinking, resulting in a lower loss factor. Moreover, it exhibits fluid-like behavior at lower frequency due to the characteristic relaxation behavior of the dynamic Si-O-B bond, resulting in a higher loss factor.

As for SSE$_{(0.85,110000)}$, it exhibits higher larger loss factor at higher frequency compared to SSE$_{(0.85,4200)}$ due to increased internal friction caused by chain entanglement. However, it shows lower loss factor compare to SSE$_{(0.85,4200)}$ at lower frequencies, which is attribute to the few density of dynamic crosslinking.

For SSE-0.85-110k, it not only possesses a relatively high density of dynamic crosslinking but also enhanced chain entanglement. Therefore, SSE-0.85-110k exhibits excellent damping property (tan $\delta > 0.3$) over a broad frequency (0.01 Hz-50 Hz) and temperature range (-20 °C-140 °C).

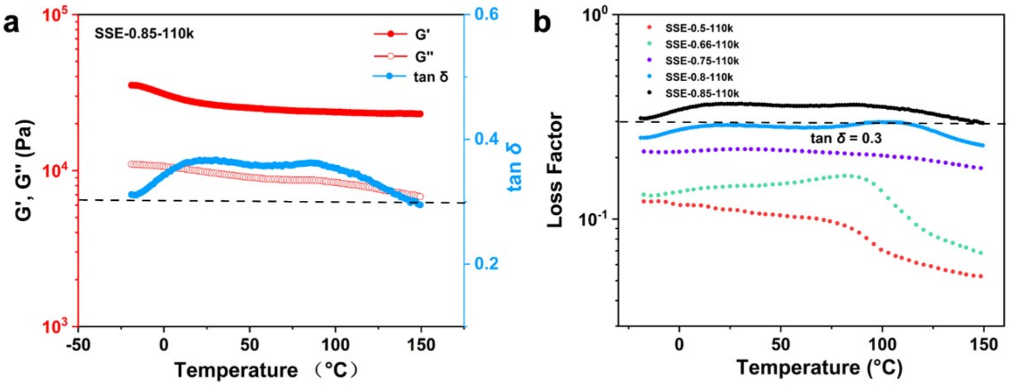

Fig. S22 (a)Temperature−sweep rheological curves of SSE-0.85-110k from -20 to 150 °C. (b) Temperature dependence of loss factor for SSE-x-110k.

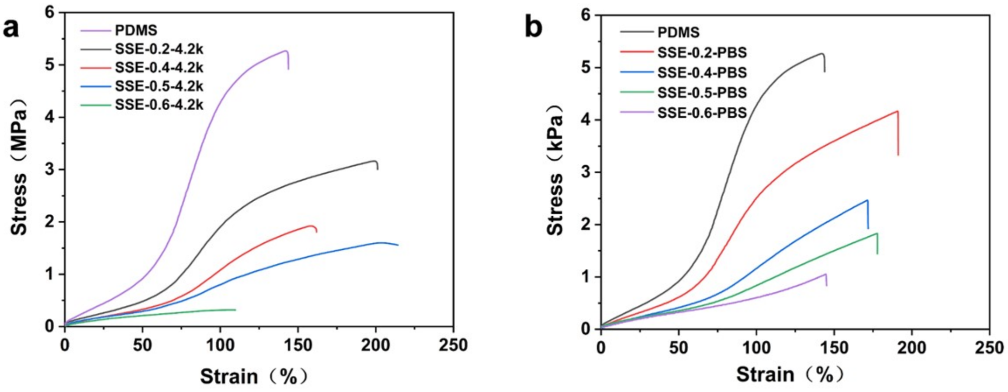

Fig. S23 Tensile stress–strain curves of SSE-x-4.2k (a) and SSE-x-PBS (b) at a strain rate of 200 mm/min. The introduction of permanent crosslinked PDMS network enhanced the mechanical strength of the elastomer.

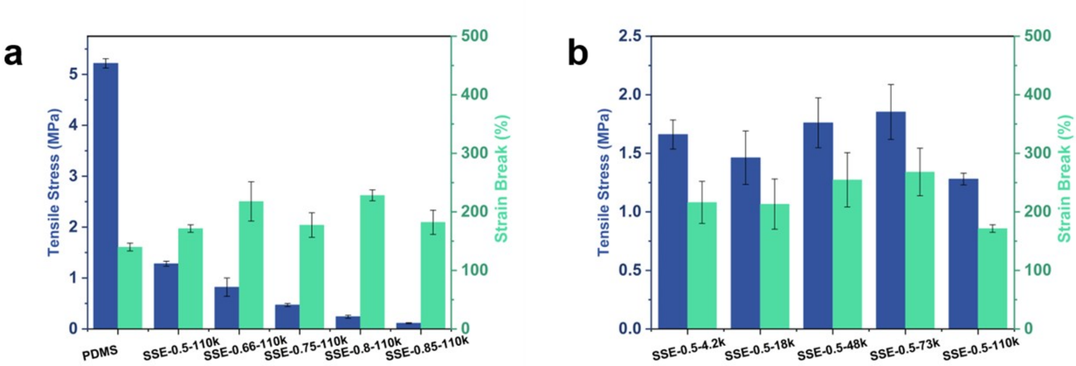

Fig. S24 a. Tensile stress and Strain break of SSEs with varied contents of PPDBS-110k. **b.** Tensile stress and Strain break of SSEs with constant PDMS content (50% w/w) but varying structure. (Error bars: SD, n = 3)

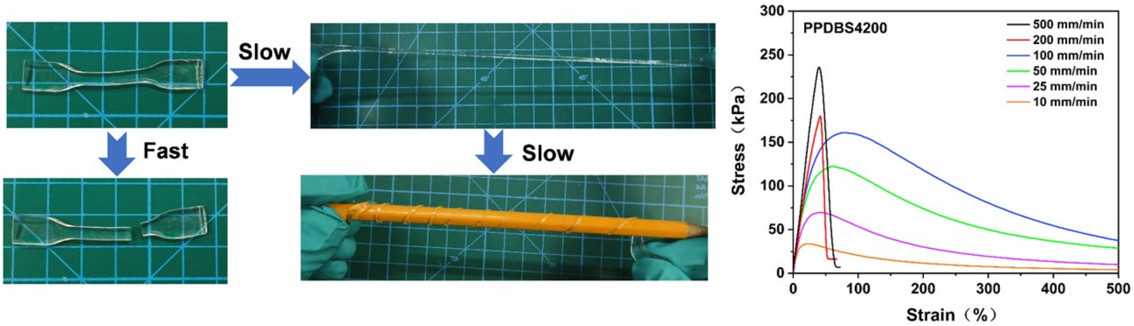

Fig. S25 Tensile stress-strain curves of PPDBS4200 under different strain rates.

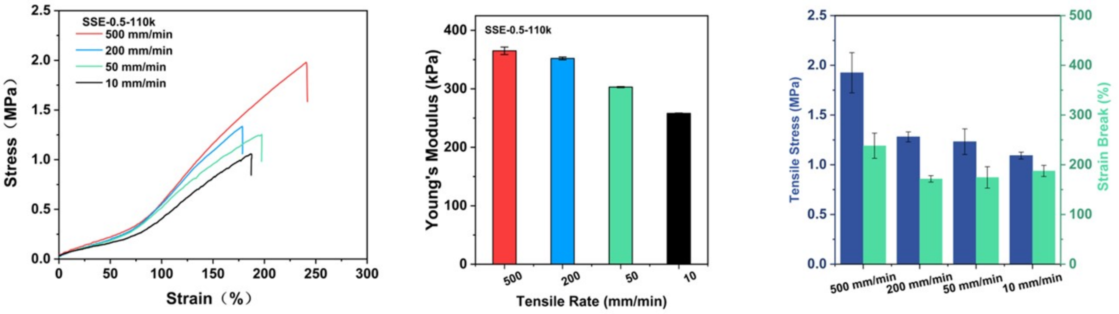

Fig. S26 Tensile stress-strain curves, corresponding Young’s moduli of SSE-0.5-110k

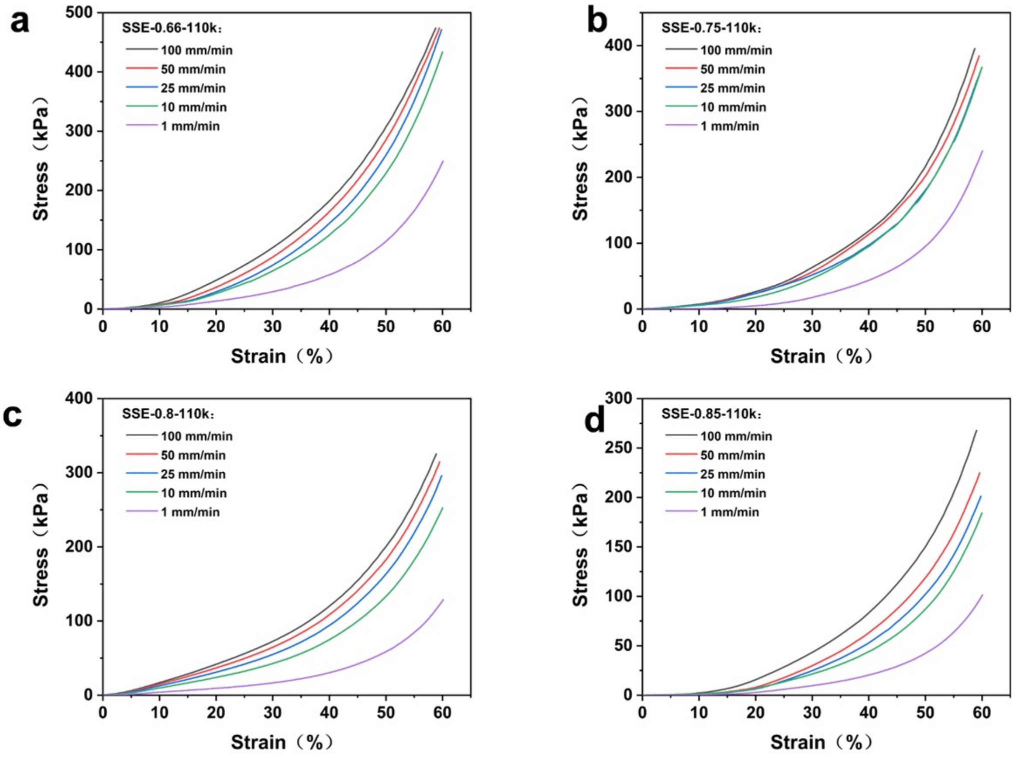

Fig. S27 Compressive stress-strain curves of SSE-0.66-110k (a), SSE-0.75-110k (b), SSE-0.8-110k (c) and SSE-0.85-110k (d) under different strain rates.

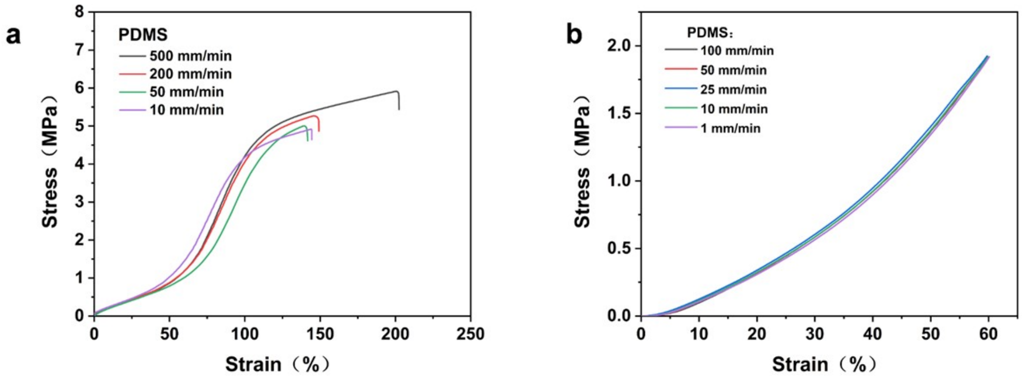

Fig. S28 Tensile (a) or compressive (b) stress-strain curves of PDMS under different strain rates.

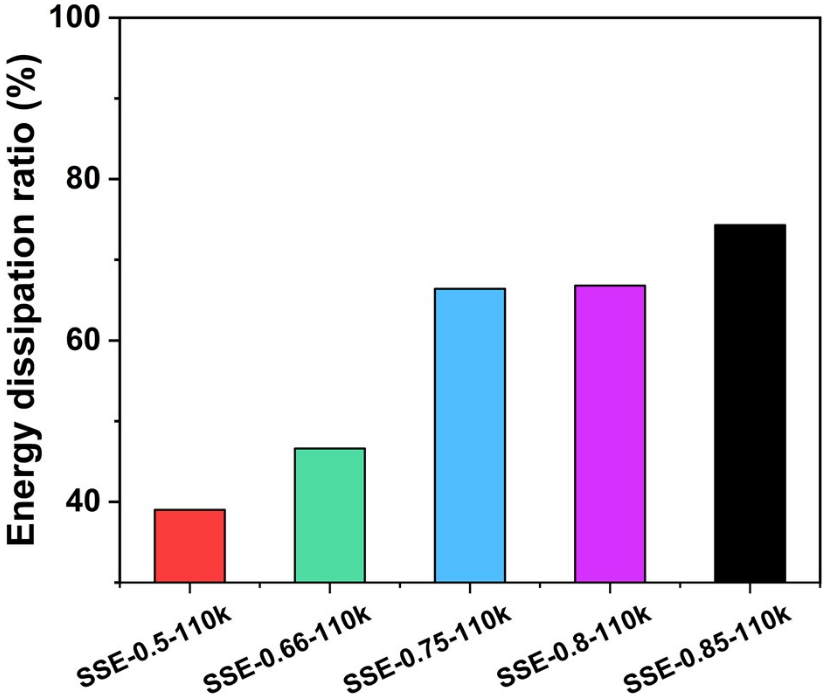

Fig. S29 Tensile strain dependent energy dissipation of SSE-x-110k.

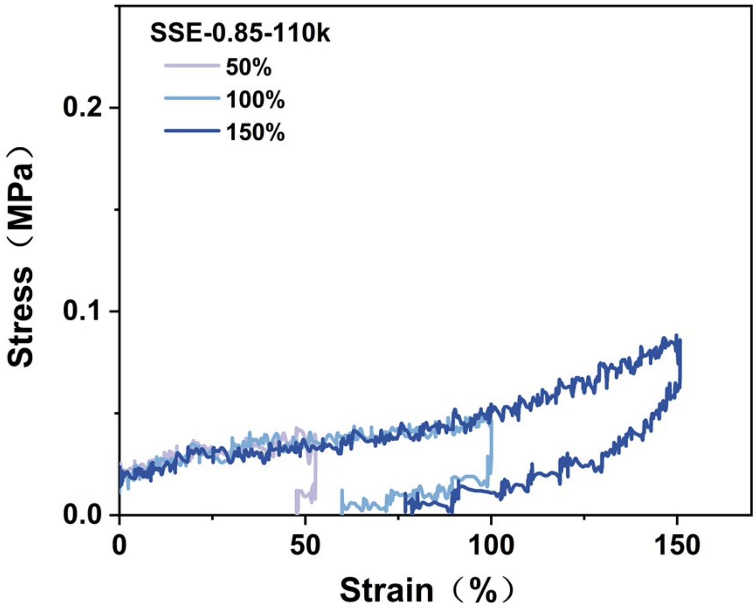

Fig. S30 Cyclic loading–unloading tensile curves of the SSE-0.85-110k at increasing strain

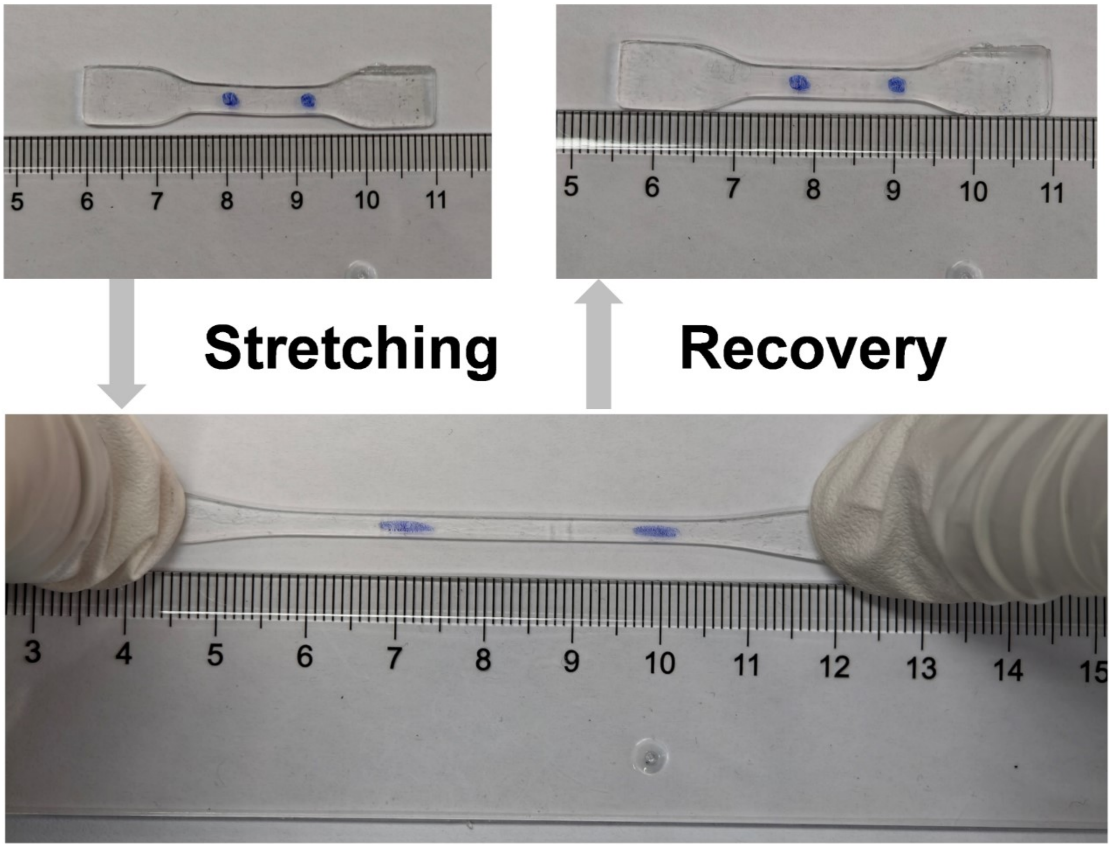

Fig. S31 Photographs demonstrating that SSE-0.5-110k can stretch 2 times and recover to its original shape.

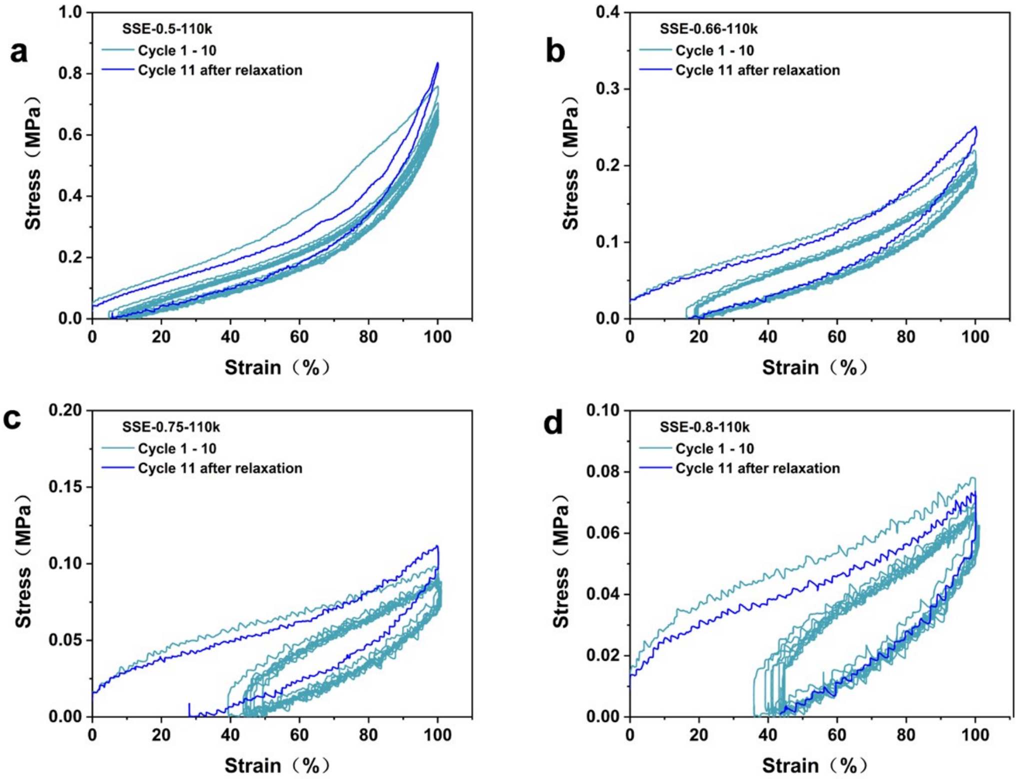

Fig. S32 Ten consecutive cyclic tensile curves of **SSE-0.5-110K (a), SSE-0.66-110k (b) and SSE-0.75-110k (c)** at 100% strain, the second tensile started at 30 s intervals; Ten consecutive cyclic tensile curves of **SSE-0.8-110k (d)** at 100% strain, the second tensile started at 60 s intervals.

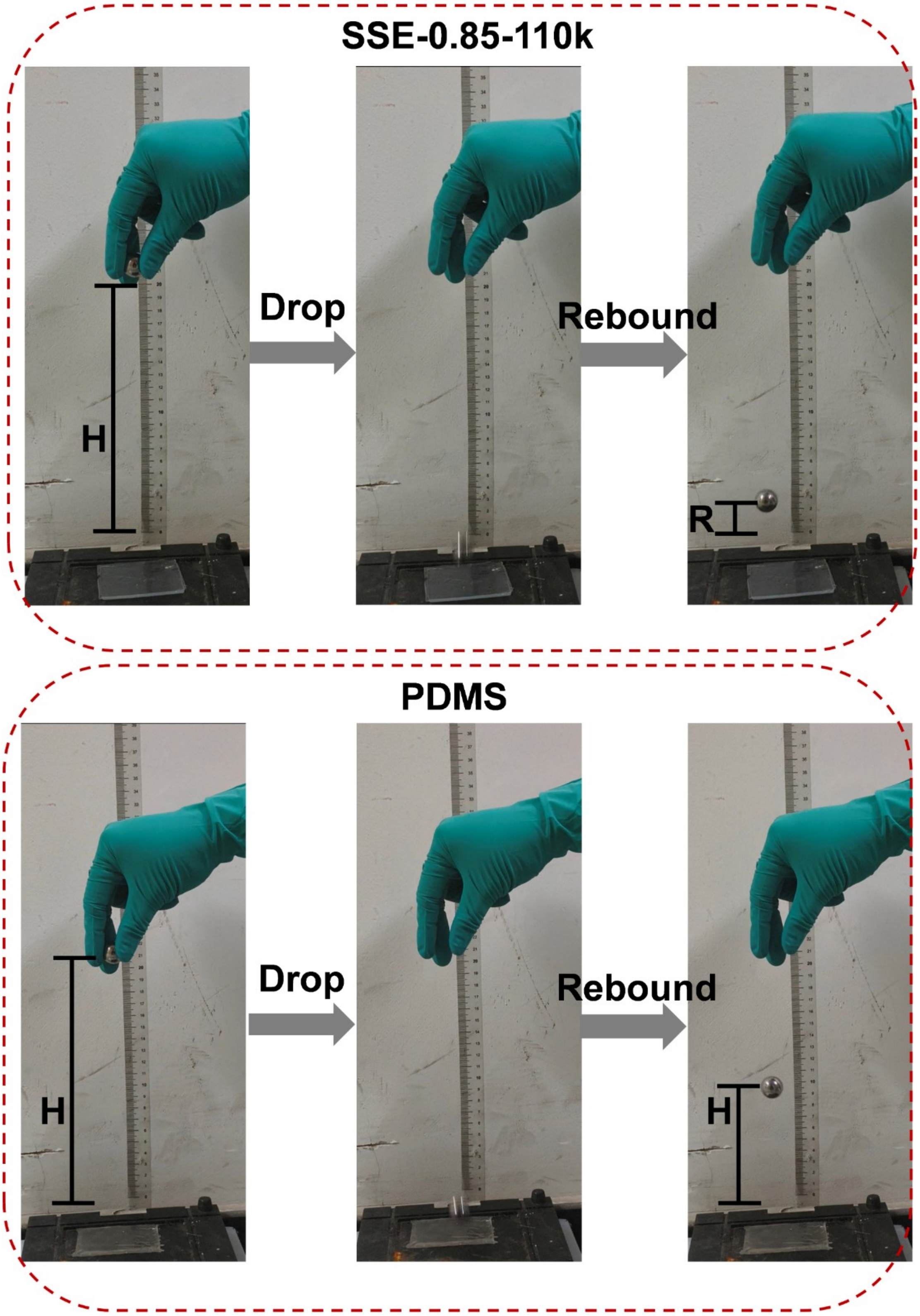

Fig. S33 Digital photographs of free-falling experiment, showing the falling and rebounding of a steel ball onto SSE-0.85-110k (top) and PDMS (bottom), respectively.

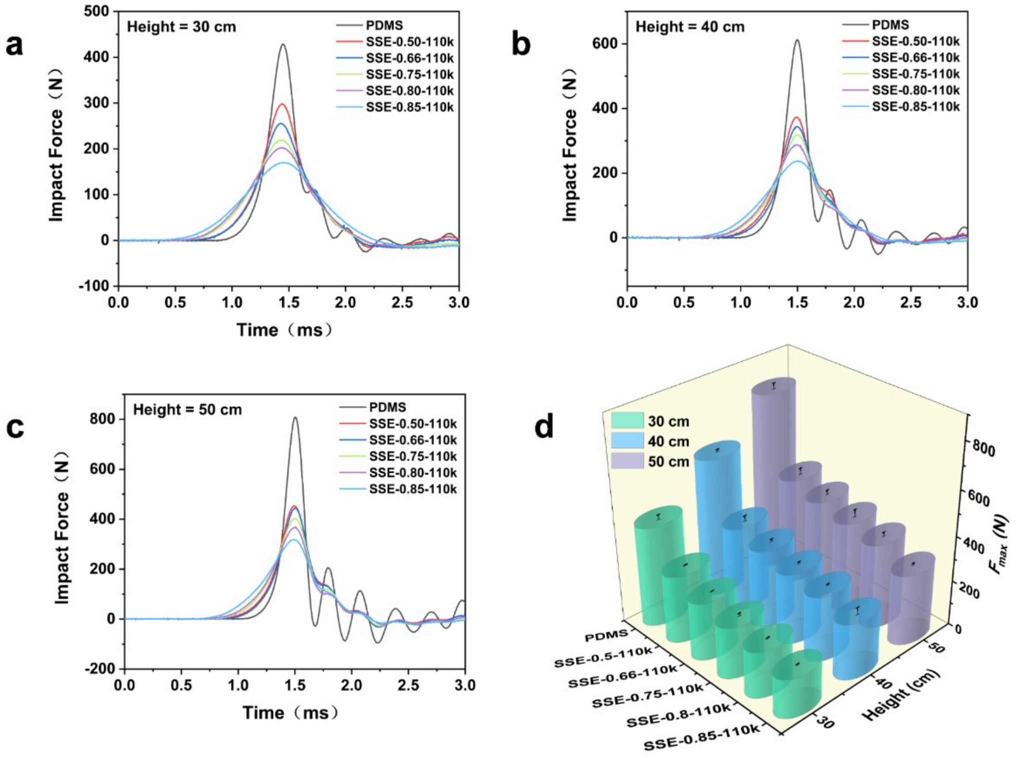

Fig. S34 Force-time curves of PDMS, SSE-0.50-110k, SSE-0.66-110k, SSE-0.75-110k, SSE-0.80-110k and SSE-0.85-110k during the falling ball impact tests when the ball dropped from heights of **30 cm (a), 40 cm (b), and 50 cm (c)**.

(d). Maximum impact force SSE-x-110k when impacted at different heights.

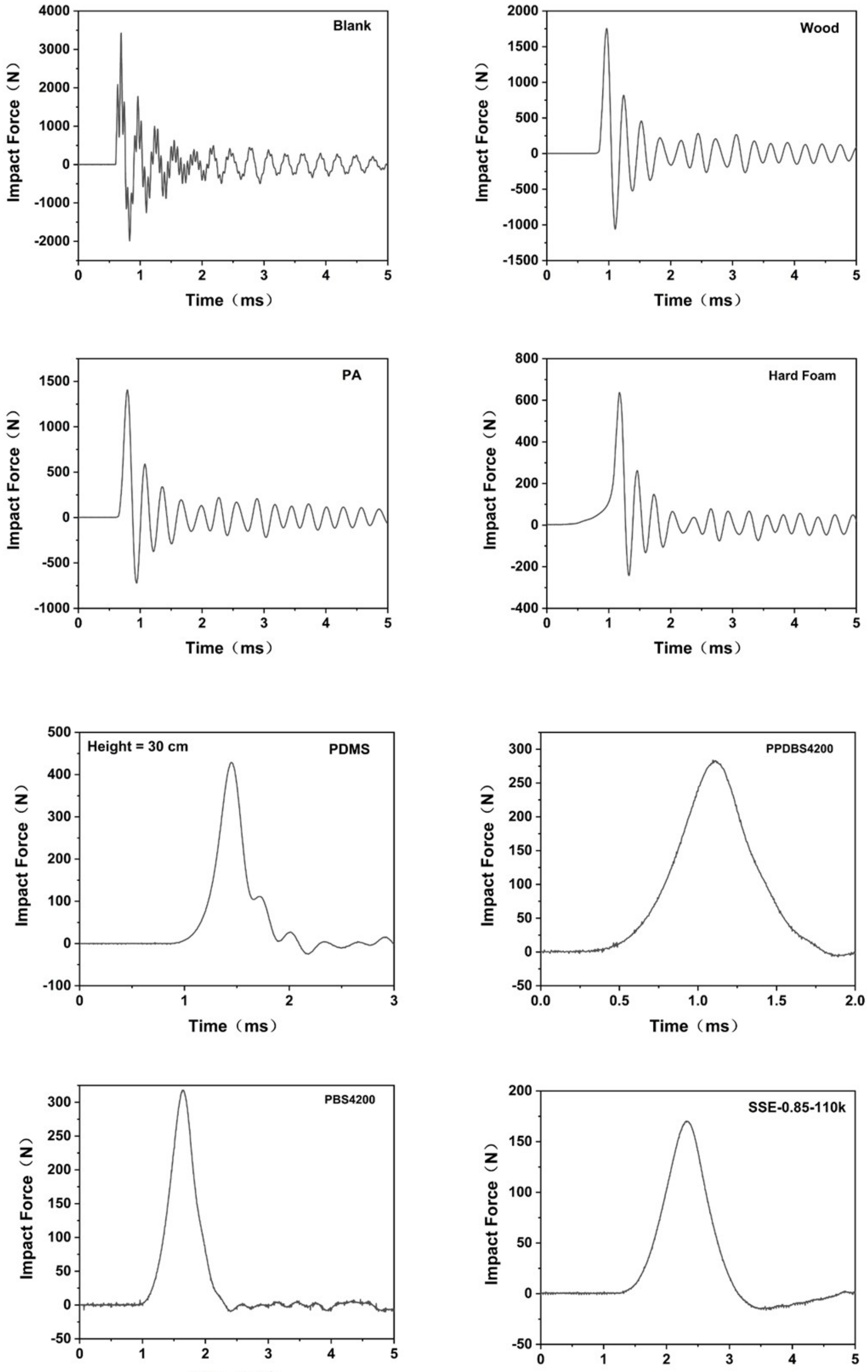

Fig. S36 Force–time curves of SSE-0.85-110k, PPDBS, PBS and common protection materials in falling ball impact tests.

Table S1: Initial Ingredients of the PPDBS and PBS

Sample	PDMS1.2k (g)[a]	PDMS4.2k (g)[a]	PDMS18k (g)[a]	PDMS36k (g)[a]	PDBA (g)	BA (g)
PPDBS1200	10	0	0	0	0.69	0
PPDBS4200	0	10	0	0	0.218	0
PPDBS36000	0	0	0	10	0.034	0
PBS1200	10	0	0	0	0	0.34
PBS4200	0	10	0	0	0	0.108
PBS18000	0	0	10	0	0	0.027
PBS36000	0	0	0	10	0	0.017

a. M_n of the PDMS-OH was Calculated by GPC

Table S2: Initial Ingredients of the PPDBS-X

Sample	PDMS 4.2k (g)[a]	PDMS 18k (g)[a]	PDMS 49k (g)[a]	PDMS 77k (g)[a]	PDMS[a] 110k(g)	PDBA (g)
PPDBS49000	0	0	5	0	0	0.012
PPDBS110000	0	0	0	0	5	0.005
PPDBS-18k	3	3	0	0	0	0.065
PPDBS-49k	3	0	3	0	0	0.065
PPDBS-77k	3	0	0	3	0	0.065
PPDBS-110k	2	0	0	0	4	0.044

a. M_n of the PDMS-OH was Calculated by GPC

Table S3: The proportion of components of SSE-x-y. (x = the weight fraction of the PPDBS)

Sample	Proportion (%)				
	PDMS	PPDBS-18k	PPDBS-49k	PPDBS-77k	PPDBS-110k
SSE-0.5-18k	50	50	0	0	0
SSE-0.5-49k	50	0	50	0	0
SSE-0.5-77k	50	0	0	50	0
SSE-0.4-110k	40	0	0	0	60
SSE-0.5-110k	50	0	0	0	50
SSE-0.66-110k	34	0	0	0	66
SSE-0.75-110k	25	0	0	0	75
SSE-0.8-110k	20	0	0	0	80

Table S4: The proportion of components of SSE-x (x = the weight fraction of the PPDBS4200 or PBS4200)

Sample	Proportion (%)		Sample	Proportion (%)	
	PDMS	PPDBS4200		PDMS	PBS4200
SSE-0.2-4.2k	80	20	SSE-0.2-PBS	80	20
SSE-0.4-4.2k	60	40	SSE-0.4-PBS	60	40
SSE-0.5-4.2k	50	50	SSE-0.5-PBS	50	50
SSE-0.6-4.2k	40	60	SSE-0.6-PBS	40	60

Supplementary References

[1] L. Porath, J. Huang, N. Ramlawi, M. Derkaloustian, R. H. Ewoldt, C. M. Evans, *Macromolecules* **2022**, 55, 4450.

[2] J. Lee, B. B. Jing, L. E. Porath, N. R. Sottos, C. M. Evans, *Macromolecules* **2020**, 53, 4741.

[3] J. Huang, Y. Xu, S. Qi, J. Zhou, W. Shi, T. Zhao, M. Liu, *Nat. Commun.* **2021**, 12, 3610.